Available online at www.sciencedirect.com

ScienceDirect

MATTER AND RADIATION AT EXTREMES

Matter and Radiation at Extremes 2 (2017) 69–76

www.journals.elsevier.com/matter-and-radiation-at-extremes

Research Article

P2 asymmetry of Au's M-band flux and its smoothing effect due to high-Z ablator dopants

Yongsheng Li [a,b,*], Chuanlei Zhai [a], Guoli Ren [a], Jianfa Gu [a], Wenyi Huo [a], Xujun Meng [a], Wenhua Ye [a,c], Ke Lan [a,c,d], Weiyan Zhang [e]

[a] *Institute of Applied Physics and Computational Mathematics, Beijing 100094, China*
[b] *Graduate School, China Academy of Engineering Physics, Beijing 100088, China*
[c] *Center for Applied Physics and Technology, Peking University, Beijing 100871, China*
[d] *Collaborative Innovation Center of IFSA, Shanghai Jiao Tong University, Shanghai 200240, China*
[e] *China Academy of Engineering Physics, Mianyang 621900, China*

Received 20 August 2016; revised 2 December 2016; accepted 5 December 2016
Available online 27 December 2016

Abstract

X-ray drive asymmetry is one of the main seeds of low-mode implosion asymmetry that blocks further improvement of the nuclear performance of "high-foot" experiments on the National Ignition Facility [Miller et al., Nucl. Fusion 44, S228 (2004)]. More particularly, the P2 asymmetry of Au's M-band flux can also severely influence the implosion performance of ignition capsules [Li et al., Phys. Plasmas 23, 072705 (2016)]. Here we study the smoothing effect of mid- and/or high-Z dopants in ablator on Au's M-band flux asymmetries, by modeling and comparing the implosion processes of a Ge-doped ignition capsule and a Si-doped one driven by X-ray sources with P2 M-band flux asymmetry. As the results, (1) mid- or high-Z dopants absorb hard X-rays (M-band flux) and re-emit isotropically, which helps to smooth the asymmetric M-band flux arriving at the ablation front, therefore reducing the P2 asymmetries of the imploding shell and hot spot; (2) the smoothing effect of Ge-dopant is more remarkable than Si-dopant because its opacity in Au's M-band is higher than the latter's; and (3) placing the doped layer at a larger radius in ablator is more efficient. Applying this effect may not be a main measure to reduce the low-mode implosion asymmetry, but might be of significance in some critical situations such as inertial confinement fusion (ICF) experiments very near the performance cliffs of asymmetric X-ray drives.

PACS Codes: 52.57.-z; 52.57.Fg; 47.20.Ma

Keywords: Inertial confinement fusion; Implosion; Low-mode distortion; M-band flux asymmetry; High-Z dopant

1. Introduction

In X-ray drive inertial confinement fusion (ICF) [1–3], high power (~500 TW) laser beams of several mega-joules are irradiated into a hohlraum made of high-Z materials (e.g. Au), on the inner wall of which they are absorbed and converted into thermal X-rays, therefore creating a high temperature (~300 eV) radiation field. The radiation field heats and ablates the outer surface of a tiny capsule placed at center of the hohlraum. The capsule is comprised of a spherical low-Z material (e.g. plastic, high density carbon, and beryllium) shell, lined with a frozen deuterium–tritium (DT) fuel layer and filled with cryogenic DT gas in its interior. The ablation produces a rocket-like reaction force that implodes the shell

* Corresponding author. Institute of Applied Physics and Computational Mathematics, Beijing 100094, China.
E-mail address: li_yongsheng@iapcm.ac.cn (Y.S. Li).
Peer review under responsibility of Science and Technology Information Center, China Academy of Engineering Physics.

http://dx.doi.org/10.1016/j.mre.2016.12.001

spherically to extremely high velocities (>350 km/s). The imploded shell compresses the DT fuel to form a hot spot of very high temperature and density, surrounded with a cooler but much denser fuel shell. The hot spot's temperature is generally sufficiently high to trigger thermal nuclear fusions; and if large enough the hot spot will be further heated by fusion releasing high energy α-particles, initiating a self-sustainable thermonuclear burn wave into the surrounding DT shell. If the confinement by inertia of the surrounding shell is long enough, the burn wave will release more energy than the lasers driving the implosion, which would be a milestone called "ignition" and has been pursued for decades by the ICF community.

The National Ignition Facility (NIF) [4] in U.S.A. is the largest laser system in the world, and has been built in 2009 to demonstrate the ignition of controlled DT-fusion, but hasn't achieved this goal yet. Low-mode asymmetric implosion is deemed one of the main mechanisms [5,6] that lead to the failure of National Ignition Campaign (NIC) [7,8] ignition experiments and to the performance degradation of subsequent "high-foot" experiments [9–13]. The low-mode shape distortion of the imploding shell [12,14], especially the in-flight P2 and P4 asymmetries, inhibited the capsule from uniform deceleration by the hot spot, reducing the transfer of shell's kinetic energy to hot spot's internal energy, thus inefficiently heating the hot spot.

There are multiple potential perturbation seeds in ICF implosion experiments that can induce the low-mode asymmetries, including the radiation flux asymmetry [15,16] in the hohlraum, capsule imperfections, the capsule support tent [17,18], the fill tube, and offset of the capsule's position in the hohlraum. Many theoretical and experimental efforts [6,15–19] have been made to investigate their effects on the implosion performance. Here we talk about another possible low-mode seed, i.e., the asymmetry of Au's M-band Flux (MFA) in high power laser heated cylindrical gold hohlraum. In such a hohlraum, much stronger M-band flux emits from laser spots than from non-laser heated wall areas, implying quite different spectra of X-ray flux incident on different areas of the capsule even if amounting equally. Moreover, the angular dependence of M-band emission [20,21] from hohlraum wall may also contribute to MFA. The first direct measurement of MFA in gold hohlraums was reported by Qi Li et al. [22], performed recently on Shenguang II laser facility showing marked P2 MFA.

It has already been proved that preheating from Au's M-band flux can both harm the stability of DT-ice/ablator interface in single shell ignition capsules [23], and exert adverse influence on double-shell implosions [24]. The effects of MFA on double-shell implosions were preliminarily addressed by Varnum and his collaborators [25]. Our previous work [26] shows that the effects of P2 MFA are of significance to asymmetric implosions of single-shell capsules. Positive P2 MFAs result in negative P2 asymmetries of hot spots and positive P2 asymmetries of shell's ρR in the acceleration phase. These P2 asymmetries of the imploding capsule will be seriously amplified by Rayleigh–Taylor (RT) [27,28] and Richtmyer–Meshkov (RM) [29,30] hydro-instabilities during the deceleration phase, therefore leading to performance degradation or even the failure of ignition if the P2 amplitude of MFA is sufficiently large.

Usually, X-ray drive asymmetry is smoothed partially by the geometric smoothing effects [1,3,31], i.e., by increasing the case-to-capsule ratio (CCR) of the cylindrical hohlraum. Clark et al. [32] and Gu et al. [33] have proposed, independently, shim designs of capsules to mitigate the impact of hohlraum asymmetries. A kind of spherical hohlraum design [34–37] was proposed in the hope of decreasing substantially the asymmetries of X-ray drives. In this paper, we study the smoothing effect of mid- or high-Z dopants in ablator on the MFAs, by modeling and comparing the implosion processes of a Ge-doped and a Si-doped ignition capsules driven by X-ray sources with P2 M-band flux asymmetries. According to our study, mid- or high-Z (Ge or Si) dopants absorb hard X-rays (M-band flux) and then re-emit isotropically, which helps to smooth the asymmetric M-band flux arriving at the ablation front, therefore reducing the P2 asymmetries of the imploding shell at the time of peak implosion velocity. Moreover, the smoothing effect of Ge-dopant is more remarkable than Si-dopant and placing the doped layer at a larger radius in ablator is more efficient.

The rest of this paper is arranged as follows. Sec. 2 gives brief descriptions of the ignition capsules and of the modeling methodology used in our study. The two dimensional performances of the two capsules are described in Sec. 3. And in Sec. 4, the smoothing effect of mid-/high-Z dopants in ablator is presented and compared between the Si-doped and the Ge-doped capsules. The effect of placing doped layer at a larger radius is also studied here. Finally, we discuss the results and give a summary in Sec. 5.

2. Model description

The NIC Rev5 Ge-doped capsule [23] and a larger Si-doped capsule [26] are considered for comparison in this study. As shown in Fig. 1(a), the capsules are composed of spherical Ge- or Si-doped polystyrene (CH) shells (or ablator), lined with layers of DT ice and containing cryogenic DT gas in their interiors. The larger radius of the Si-doped capsule can help to absorb more X-ray energy, and its thicker shell can help to reduce the coupling between the ablation front and the fuel/ablator interface, thus mitigating the growth rate of hydro-instability.

The corresponding X-ray drives for the two capsules are plotted in Fig. 1(b), with the solid lines showing the equivalent radiation temperature and the dashed lines showing the M-band fraction. The black lines are for the Ge-doped capsule, taken from Ref. [23] and temporally re-shaped in our simulations to produce the optimal Munro shock timing [38], and the red lines are for the Si-doped capsule, taken from Ref. [26]. The latter is a three-step 302 eV pulse shape, and its foot is a bit higher than the former but lower than the "high-foot" experiments [11] on NIF, which leads to an in-flight DT adiabat of about 1.14 and consequently helps to restrain the growth rate of hydro-instability.

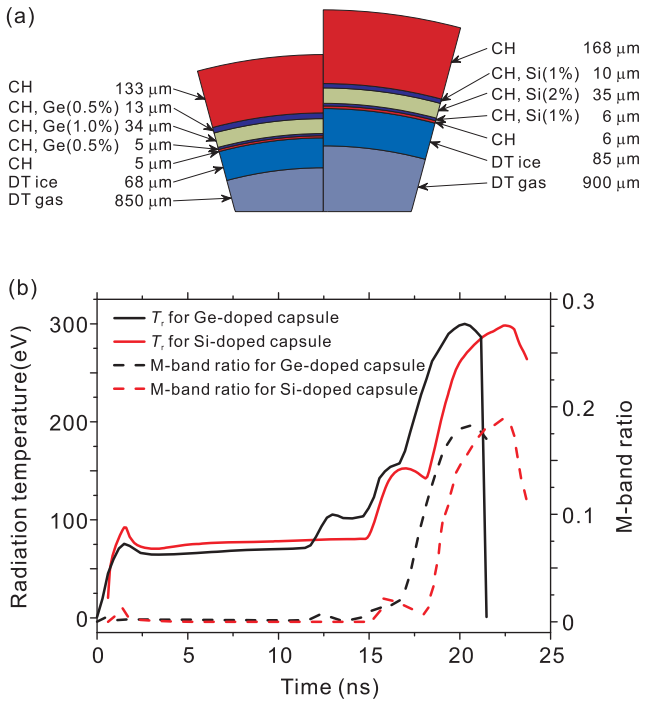

Fig. 1. (a) Pie diagram of the ignition capsules in this study and (b) X-ray sources driving the capsule. The solid lines show the equivalent radiation temperature and dashed lines show the M-band fraction of the X-ray drives, black for the Ge-doped capsule and red for the Si-doped capsule.

Here, we focus on the capsules' low-mode hydro-instabilities induced by the MFA of X-ray drives and mainly talk about the smoothing effects of mid-/high-Z dopants in ablator on MFAs just before the ablation fronts. So we list some one dimensional performance parameters of the two capsules in Table 1 for references (note: 1 Gbar = 10^8 MPa).

Two radiation hydrodynamic codes, i.e., LARED-IC [39] and LARED-S [40,41], are used consecutively to perform the two dimensional (2D) capsule-only simulations. The former code is based on Lagrangian meshes in a cylindrical geometry, including modules for multi-grouped radiation transfer where the discrete-ordinate method [42] is implemented, and the flux-limited Spitzer–Harm thermal conduction for both electrons and ions. It is used here to model the first stage of X-ray driven implosion processes of the capsules, including the application of asymmetric X-ray drives, the ablation as well as the acceleration process of capsules' shell. When the shell arrives at the peak implosion velocity or the X-ray drive finishes, the modeling is taken over by the latter code to perform simulations of the second stage of capsules' implosion processes. LARED-S has been widely used in the studies of hydro-instability [43–47], and it is based on Eulerian meshes in a spherical geometry and includes modules for multi-grouped radiation diffusion, electron and ion thermal conduction using the same model as the former code, DT nuclear fusion, and multi-grouped alpha particle diffusion. The material opacities used in our simulations are tabulated from our OPINCH [48] code where the relativistic Hartree–Fock–Slater (HFS) self-consistent average-atom model is embedded, and equation of state (EOS) data are patched from several physical models and smoothed in the transition regions by interpolation.

Table 1
Some 1D implosion parameters of the capsules showed in Fig. 1(a).

	[a]Ge-doped	[b]Si-doped
Radiation temperature (eV)	300	302
Implosion velocity (km/s)	370	348
In-flight fuel adiabat	0.83	1.14
In-flight shell thickness (μm)	35	45
ITF1D[c]	7.23	3.86
Yield (MJ)	17.5	20.3
Fuel areal density (g/cm^2)	1.43	1.34
Stagnation pressure (non-α) (Gbar)	405	391
Convergence ratio (with-α)	35	37
Absorbed energy by capsule (kJ)	162	202

[a] Data for Ge-doped capsule are from 1-D RDMG [42] simulation.
[b] Data for Si-doped capsule are from Ref. [26].
[c] One dimensional ignition threshold factor.

The benefits of this collaboration have been discussed in Ref. [26], among which eliminating the non-physical smoothing of X-ray drive asymmetry introduced by the diffusion approximation of radiation transfer in code LARED-S is vital to our study here. Thus, without the non-physical smoothing brought by numerical method, the smoothing effect from our simulations is mainly caused by the geometrical smoothing factor [1,3,31] and the physical processes, such as X-ray emission, absorption, and transfer. Since the geometrical smoothing effect can be calculated analytically [1,3,31], it's easy to isolate the physical ingredient in our numerical studies of smoothing effects on MFAs.

In the LARED-IC simulations, the X-ray drives are applied onto a capsule-concentric spherical surface at a radius of 3000 μm. Low density (~1.0×10^{-4} g/cm^3) CH foam is filled in the space between the capsule and the supposed spherical surface. The X-rays are divided into 30 groups, ten of which are used to resolve Au's M-band ($h\nu > 1.8$ keV) flux. The spectrum of X-ray drive is constructed [49,50] by overlapping a Gaussian bump spanning Au's M-band onto the Planckian spectra. The influence of the M-band real spectra [51,52] will be further studied in the future. For the sake of simplicity, (1) the MFAs during the first two/three steps of X-ray drives are elided due to their very small fractions of M-band flux as shown in Fig. 1(b); (2) only the P2 components of M-band flux asymmetry is taken into account, since the P4 and higher modes are negligible both due to the smaller amplitudes of these perturbations and the much stronger geometric smoothing effects [1,3,31] on these modes; and (3) constant P2 asymmetries are applied to the M-band flux in our simulations, since it seems that only the time-integrated asymmetry matters [32]. These simplifications will not change our conclusions. The P2 asymmetry of M-band flux is applied according to the formula, $I_{\mathrm{M-band}}(\theta) = \frac{\sigma T_r^4}{2\pi} f_{\mathrm{M-band}}(\theta) = \frac{\sigma T_r^4}{2\pi}(a_0 \mathrm{P}_0 + a_2 \mathrm{P}_2 \cos\theta)$, where σ is Stefan–Boltzmann constant, P_0 and P_2 are fully normalized Legendre polynomials, $a_0\mathrm{P}_0$ is the 4π-averaged M-band flux fraction as shown by the dashed lines in Fig. 1(b),

and constant P2 asymmetry means a_2/a_0 does not vary with time.

In our study, the spectrally integrated total flux incident onto the capsule is kept symmetric while applying P2 MFAs to X-ray drives. This introduces anti-phase P2 asymmetries of softer ($h\nu > 1.8$ keV) X-ray drive, the magnitudes of which can be calculated by formula $\left(\frac{P_2}{P_0}\right)_{\text{low-frequency}} = -\left(\frac{P_2}{P_0}\right)_{\text{M-band}} \frac{f_{M0}(t)}{1-f_{M0}(t)}$ with f_{M0} being 4π-averaged M-band fraction as shown by the dashed lines in Fig. 1(b). The influence of anti-phase P2 asymmetries of softer X-ray has been discussed in Ref. [26], i.e., counteracting partially the effect of the related P2 MFA.

3. Effects of MFA on 2D performances of doped capsules

The content of M-band flux in X-ray drives can strongly influence the capsules' ablation and implosion processes [50]. Generally, the M-band flux can easily penetrate the ablation front and preheat the inner ablator materials, thus significantly enhance the ablation rate and acceleration of the imploding shell. If X-ray drives with positive P2 asymmetric M-band flux are applied to the capsules, the shells will move faster in the polar direction than in the equatorial direction, forming hot spots and shells of negative P2 asymmetries at the time of peak implosion velocity. These P2 perturbation will be further amplified by the RT instability growth during deceleration phases.

Fig. 2 shows the 2D simulation results of the two capsules both at the time of peak implosion velocity and the stagnation time, with the P2 amplitudes of MFAs being $a_2/a_0 = 10\%$. The left side of each panel corresponds to the distribution of ion temperature, and the right side shows the fluid density. The black lines show the fuel/ablator interfaces, and the white lines are the boundaries of hot spots defined by the 1-keV contours of ion temperature. Apparently, the shapes of both the hot spots and the shells are negatively P2 asymmetric, while the asymmetries of fuel areal density are not so remarkable.

Decomposing the flow fields into Legendre polynomials, we get the a_2/a_0 amplitudes of the ablation front shapes, the hot spot shapes, and the fuel areal densities for the two capsules at the time of peak implosion velocity. The first two are positive while the third one is negative, but all three increase linearly with a_2/a_0 amplitudes of MFAs as shown in Fig. 3(a). As for the P2 perturbations at stagnation times of the two capsules, we plot their a_2/a_0 amplitudes of hot spot shapes and fuel areal densities in Fig. 3(b), which were greatly amplified during the deceleration stage via ablative Rayleigh–Taylor hydro-instability (RTI) [27,28] and Bell–Plesset effects [53–56].

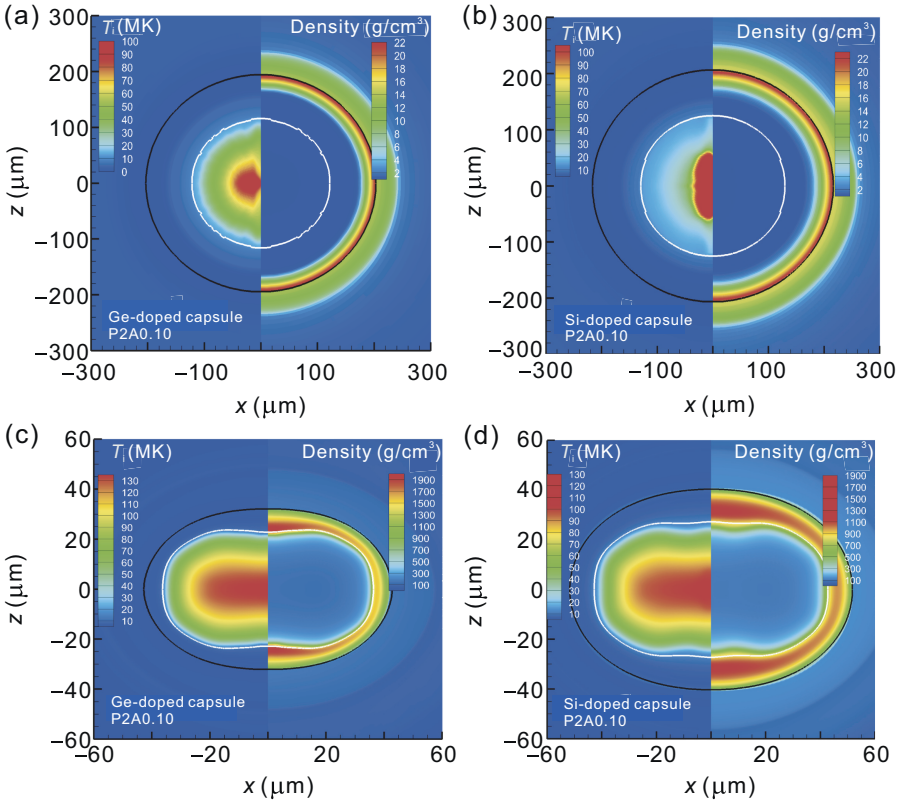

Fig. 2. Ion temperature (left half of each panel) and density (right half of each panel) distributions for (a), (c) Ge-doped capsule and (b), (d) Si-doped capsule at (a), (b) the time of peak implosion velocities and (c), (d) stagnation time, with the a_2/a_0 amplitudes of P2 MFA being 10%. The z-axes correspond to capsules' polar direction. The black lines show the interfaces of DT fuel and CH ablator, and the white lines are the boundaries of hot spots defined by the 1-keV contours of ion temperature.

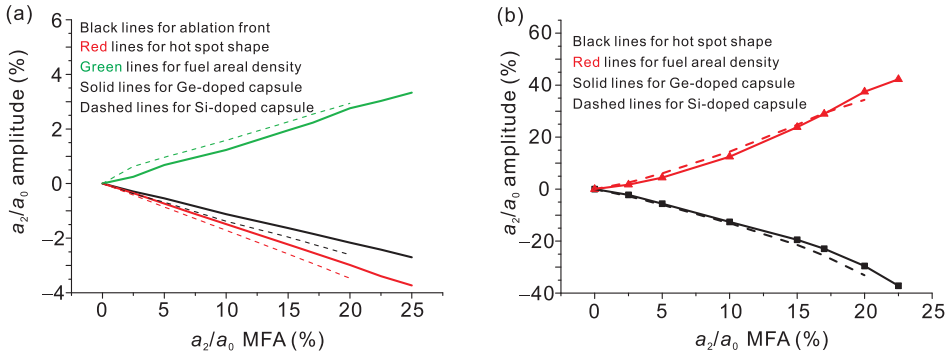

Fig. 3. (a) The a_2/a_0 amplitudes of the ablation front shapes (black lines), the hot spot shapes (red lines), and the fuel areal densities (green lines) of the two imploding capsules at peak implosion velocities, all increasing with the a_2/a_0 amplitudes of MFA. (b) a_2/a_0 amplitudes of the hot spot shapes (black line + marks) and the fuel areal densities (red line + marks) of the two imploding capsules at stagnation time.

As can be seen from Fig. 2(a) and (c), oblate or toroidal hot spots form at stagnation, which reduces the transformation of shell's kinetic energy to hot-spot's internal energy and cools the hot spots via enhanced electron thermal conduction due to the enlarged hot spot surfaces and vortices in them [26]. As the final result of M-band flux asymmetry, the capsules' nuclear performance degrades with the increase of the P2 amplitudes of MFAs. Fig. 4 shows the YO1Ds (Yield Over 1D performance) vs. a_2/a_0 amplitudes of MFA, with the black line plus filled squares being for the Ge-doped capsule and red line plus filled triangles for the Si-doped capsule. Steep cliffs appear around the points where a_2/a_0 amplitudes are 0.232 and 0.158 for the two capsules, respectively. Combining Fig. 4 with Fig. 3(b), we can see that the Ge-doped capsule is more robust to the P2 distortions of hot spots at stagnation than the Si-doped capsule, since the former capsule's ITF1D is much bigger than the latter as shown in Table 1.

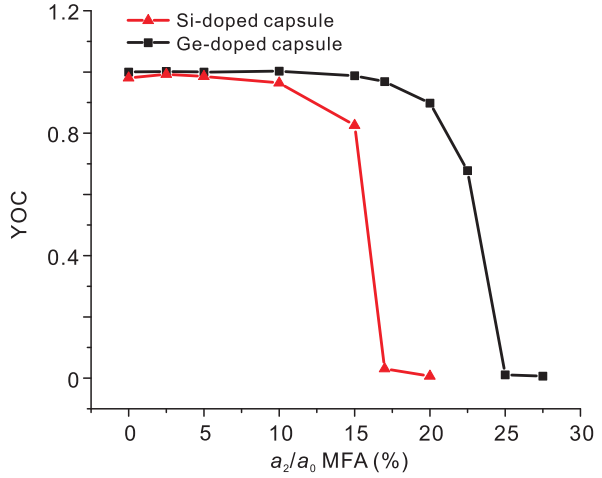

Fig. 4. Simulated nuclear performances (Yield over Clean, YOC) as functions of the a_2/a_0 amplitudes of MFA applied on an $R = 3000$ μm concentric spherical surface. The black and the red lines are for the Ge-doped and the Si-doped capsules, respectively. Steep cliffs appear near the points where a_2/a_0 amplitudes are 0.232 and 0.158, respectively.

4. Smoothing effect of high-Z dopants

In this section we study the smoothing effect of high-Z dopants on MFA. Fig. 3(a) shows that the shell's P2 distortion at the time of peak implosion velocity responds linearly to MFA and the Ge-doped capsule is more resistant to P2 MFAs than the Si-doped capsule. The difference between the responses of the two capsules to P2 MFAs is about 15% ~ 20%. It cannot be ascribed to the different initial outer radii of Ge- and Si-doped capsules, because the resultant difference of geometrical smoothing factors of MFA is calculated [31] to be less than 5%. Therefore, it should be due to the different dopants.

Basically, the main purpose of adding high-Z dopants is to absorb hard X-rays (i.e. M-band flux), therefore to mitigate the preheating of ablators adjacent to DT fuel and to lower the RT growth rate there [1,2]. To make it clearer, we present in Fig. 5 the opacities of pure CH ablator, Ge-doped and Si-doped CH ablators calculated from OPINCH [48]. As seen from Fig. 5, both doped ablators show remarkably higher Au M-band (>1.8 keV) opacity than pure CH ablator at same (ρ,T) states. This property certainly helps the cold dense ablator between

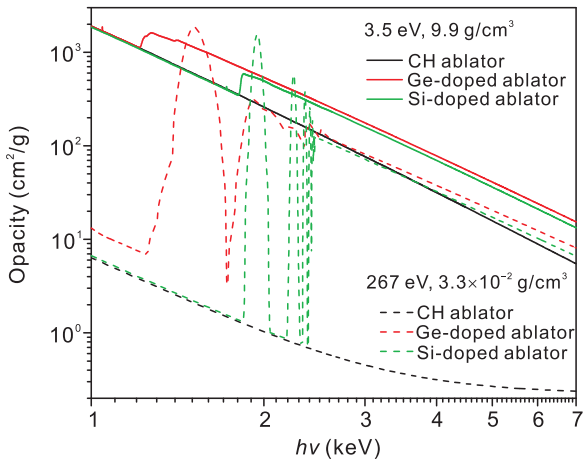

Fig. 5. Opacities of pure CH ablator, Ge-doped and Si-doped CH ablators, showing remarkably higher Au M-band (>1.8 keV) opacity of doped ablators.

the fuel/ablator interface and the ablation front to absorb much of the M-band flux traversing the ablation front. Meanwhile, it helps the ablated hot rare plasmas to absorb partially the incoming M-band flux as shown in Fig. 6(a) by the dashed lines in regions with radius <650 μm.

Part of the absorbed M-band flux is re-emitted isotropically by the hot rare plasmas, beneficial to smoothing the MFA just before the ablation front. Fig. 6(b) shows the radial distributions of a_2/a_0 MFAs for the Si-doped (green line) and the Ge-doped (red line) capsules and that without dopant's smoothing effect (black line), i.e., only the geometrical smoothing effect included. The a_2/a_0 MFA lines of both doped capsules are dropping closely along the geometrical smoothing line from radius 3000 μm to ~650 μm where pure CH plasmas is filled, while they go dramatically below the geometrical smoothing line from ~650 μm to ~350 μm where doped CH plasmas is filled, indicating the smoothing effect of high-Z dopants on MFAs. Furthermore, as clearly shown by the inset of Fig. 6(b), the fact that the Ge-doped capsule shows smaller MFA than the Si-doped capsule also confirms the smoothing effect of high-Z dopants, since the former is more opaque in Au M-band than the latter as shown in Fig. 5. When M-band flux transfers into the ablation fronts, MFAs get extraordinarily high because of the ablation fronts drastically absorbing M-band flux and of the MFA-resulted ablation-front asymmetries. The Planckian part of X-ray drives can also be smoothed by mid-/high-Z dopants, which will be studied in the future.

We performed another simulation of a variant Ge-doped capsule with the doped layer being moved outward to a radius of about 20 μm larger, while its a_2/a_0 MFA of X-ray source is the same as the original one (10%). Its a_2/a_0 amplitudes of the ablation front, the hot spot shape and the fuel areal density at the time of peak implosion velocity are −0.63%, −1.04% and 0.92%, respectively, all of which are smaller than those of model P2A0.10 as shown in Fig. 3(a). Specifically, the radial distributions of a_2/a_0 MFAs for pure geometric smoothing and the two Ge-doped capsules are plotted in Fig. 7, indicating more efficient smoothing effect for the variant Ge-doped capsule than for the original one. Apparently, by moving the doped layer to a larger radius, we brought ahead the time when the main pulse of X-ray drive began to ablate the doped layer, therefore improved the smoothing effect of high-Z dopants on MFA.

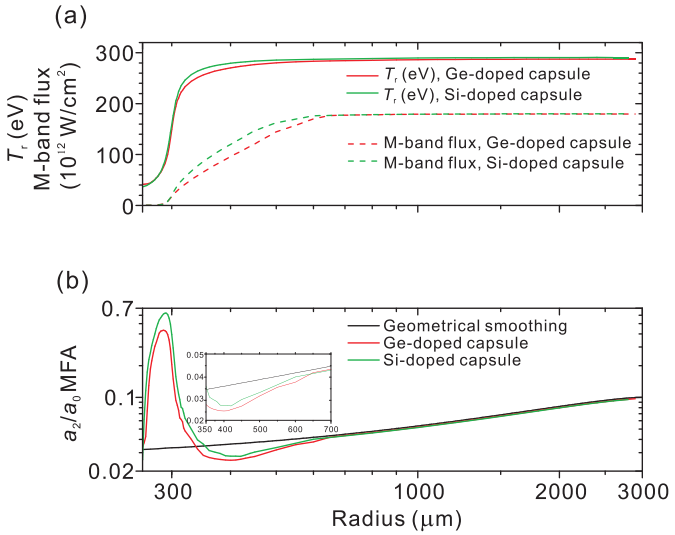

Fig. 6. The radial distributions of (a) radiation temperature and M-band flux and (b) a_2/a_0 MFAs of the Si-doped (green line) and the Ge-doped (red line) capsules and that without dopant's smoothing (black line, only the geometrical smoothing effect included). The ablation front is at ~300 μm and the interface between doped and pure CH ablator plasmas is at about 650 μm.

5. Summary and discussion

From our study, the MFA in radiation fields of laser-heated cylindrical gold hohlraums can result in low-mode implosion distortions. Positive P2 MFAs result in negative P2 asymmetries of hot spots and positive P2 asymmetries of shell's ρR at the time of peak implosion velocity, both of which increase linearly with the P2 amplitudes of MFA and are seriously amplified by the growth of RT and RM hydro-instabilities during the deceleration phase. An oblate or toroidal hot spot forms at stagnation time, leading to the degradation of nuclear performance or even the failure of ignition when the P2 amplitude of MFA is sufficiently large. The nuclear yield cliffs of the Ge- and the Si-doped capsules are obtained, locating at the points where the a_2/a_0 amplitudes are 23.2% and 15.8%, respectively.

In addition, mid-/high-Z dopants in ablators can smooth MFAs just before the ablation front, therefore mitigate the effects of MFA. By doping higher-Z materials, more dopants, or placing the doped layer to a larger radius, the smoothing effects of dopants on MFA can be enhanced, even though the implosion velocity may decrease inevitably. Mid-/high-Z dopants might not be the main method to mitigate the low-mode distortions of ICF implosions, but if combined with

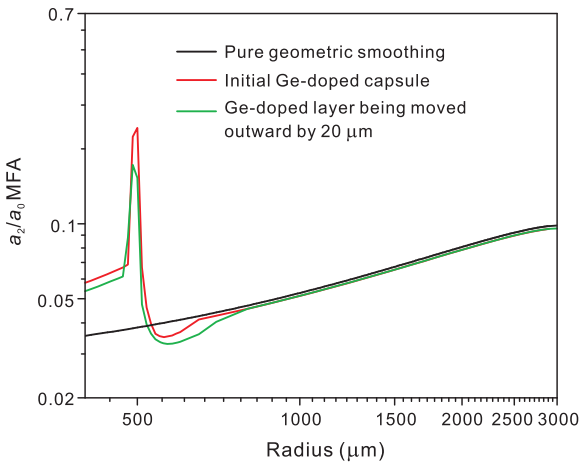

Fig. 7. The radial distributions of a_2/a_0 MFAs for pure geometric smoothing (black line), the Ge-doped (red line) capsule, and the variant Ge-doped capsule (green line) with the dopant layer being moved outward by 20 μm. These lines show the smoothing effect of dopants and more efficient smoothing of the variant Ge-doped capsule than the original one.

other approaches, it can be helpful in some situations where the performance is near the cliff and meanwhile the implosion velocity is not so critical. More efforts will be devoted to finding more efficient dopants and/or optimal doping methods in our future work.

Acknowledgments

This work is partly supported by the National Natural Science Foundation of China under Grant Nos. 11575034, 11275031, 11475033 and the Fundamental Research Program of CAEP (Contract No. 2013A0102002).

References

[1] J. Lindl, Development of the indirect-drive approach to inertial confinement fusion and the target physics basis for ignition and gain, Phys. Plasmas 2 (1995) 3933.
[2] J.D. Lindl, P. Amendt, R.L. Berger, S.G. Glendinning, S.H. Glenzer, et al., The physics basis for ignition using indirect-drive targets on the National Ignition Facility, Phys. Plasmas 11 (2004) 339.
[3] S. Atzeni, J. Meyer-ter-Vehn, The Physics of Ineritial Fusion, Clarendon, Oxford, 2004.
[4] G.H. Miller, E.I. Moses, C.R. Wuest, The National Ignition Facility: enabling fusion ignition for the 21st century, Nucl. Fusion 44 (2004) S228.
[5] D.S. Clark, D.E. Hinkel, D.C. Eder, O.S. Jones, S.W. Haan, et al., Detailed implosion modeling of deuterium-tritium layered experiments on the National Ignition Facility, Phys. Plasmas 20 (2013) 056318.
[6] D.S. Clark, M.M. Marinak, C.R. Weber, D.C. Eder, S.W. Haan, et al., Radiation hydrodynamics modeling of the highest compression inertial confinement fusion ignition experiment from the National Ignition Campaign, Phys. Plasmas 22 (2015) 022703.
[7] John Lindl, Otto Landen, John Edwards, Ed Moses, NIC team, Review of the National Ignition Campaign 2009−2012, Phys. Plasmas 21 (2014) 020501.
[8] E.I. Moses, R.E. Bonanno, C.A. Haynam, R.L. Kauffman, B.J. MacGowan, et al., The National Ignition Facility: Path to ignition in the laboratory, J. Phys. IV 133 (2006) 57.
[9] T.R. Dittrich, O.A. Hurricane, D.A. Callahan, E.L. Dewald, T. Döppner, et al., Design of a high-foot high-adiabat ICF capsule for the National Ignition Facility, Phys. Rev. Lett. 112 (2014) 055002.
[10] H.-S. Park, O.A. Hurricane, D.A. Callahan, D.T. Casey, E.L. Dewald, et al., High-adiabat high-foot inertial confinement fusion implosion experiments on the National Ignition Facility, Phys. Rev. Lett. 112 (2014) 055001.
[11] O.A. Hurricane, D.A. Callahan, D.T. Casey, E.L. Dewald, T.R. Dittrich, et al., The high-foot implosion campaign on the National Ignition Facility, Phys. Plasmas 21 (2014) 056314.
[12] A.B. Zylstra, J.A. Frenje, F.H. Seguin, J.R. Rygg, A. Kritcher, et al., In-flight observations of low-mode *R* asymmetries in NIF implosions, Phys. Plasmas 22 (2015) 056301.
[13] V.A. Smalyuk, H.F. Robey, T. Döppner, O.S. Jones, J.L. Milovich, et al., First results of radiation-driven, layered deuterium-tritium implosions with a 3-shock adiabat-shaped drive at the National Ignition Facility, Phys. Plasmas 22 (2015) 080703.
[14] T. Ma, P.K. Patel, N. Izumi, P.T. Springer, M.H. Key, et al., Thin shell, high velocity inertial confinement fusion implosions on the National Ignition Facility, Phys. Rev. Lett. 111 (2013) 085004.
[15] R.H.H. Scott, D.S. Clark, D.K. Bradley, D.A. Callahan, M.J. Edwards, et al., Numerical modeling of the sensitivity of X-ray drive implosions to low-mode flux asymmetries, Phys. Rev. Lett. 110 (2013) 075001.
[16] R.P.J. Town, D.K. Bradley, A. Kritcher, O.S. Jones, J.R. Rygg, et al., Dynamic symmetry of indirectly driven inertial confinement fusion capsules on the National Ignition Facility, Phys. Plasmas 21 (2014) 056313.
[17] R. Tommasini, J.E. Field, B.A. Hammel, O.L. Landen, S.W. Haan, et al., Tent-induced perturbations on areal density of implosions at the National Ignition Facility, Phys. Plasmas 22 (2015) 056315.
[18] S.R. Nagel, S.W. Haan, J.R. Rygg, M. Barrios, L.R. Benedetti, et al., Effect of the mounting membrane on shape in inertial confinement fusion implosions, Phys. Plasmas 22 (2015) 022704.
[19] O.A. Hurricane, D. A.Callahan, D.T. Casey, E.L. Dewald, T.T. Dittrich, et al., Inertially confined fusion plasmas dominated by alpha-particle self-heating, Nat. Phys. 12 (2016) 800−806.
[20] N.K. Gupta, V. Kumar, Angular dependence of M and N band radiation and the effect of angular anisotropy on the total conversion efficiency of X rays emitted from a laser irradiated gold foil, Laser Part. Beams 13 (1995) 389.
[21] J.-Y. Zhou, T.-X. Huang, M. Lin, W. Jiang, Angular distribution measurement and simulation of M band X-ray from the half-hohlraum, Acta Phys. Sin. 59 (2010) 1913.
[22] Q. Li, L. Yao, L.F. Jing, Z.M. Hu, C.W. Huang, et al., Fluorescence based imaging for M-band drive symmetry measurement in hohlraum, Phys. Plasmas 23 (2016) 112707.
[23] S.W. Haan, J.D. Lindl, D.A. Callahan, D.S. Clark, J.D. Salmonson, et al., Point design targets, specifications, and requirements for the 2010 ignition campaign on the National Ignition Facility, Phys. Plasmas 18 (2011) 051001.
[24] P.A. Amendt, H.F. Robey, H.-S. Park, R.E. Tipton, R.E. Turner, et al., Hohlraum-driven ignition-like double-shell implosions on the Omega Laser Facility, Phys. Rev. Lett. 94 (2005) 065004.
[25] W.S. Varnum, N.D. Delamater, S.C. Evans, P.L. Gobby, J.E. Moore, et al., Progress toward ignition with noncryogenic double-shell capsules, Phys. Rev. Lett. 22 (2000) 5153.
[26] Y.S. Li, J.F. Gu, C.S. Wu, P. Song, Z.S. Dai, et al., Effects of the P2 M-band flux asymmetry of laser-driven gold hohlraums on the implosion of ICF ignition capsule, Phys. Plasmas 23 (2016) 072705.
[27] L. Rayleigh, Scientific Papers II, Cambridge University Press, Cambridge, England, 1900, p. 200.
[28] G. Taylor, The instability of liquid surfaces when accelerated in a direction perpendicular to their planes, Proc. R. Soc. Lond. Ser. A 201 (1950) 192.
[29] R.D. Richtmyer, Taylor instability in shock acceleration of compressible fluids, Commun. Pure Appl. Math. 13 (1960) 297.
[30] E.E. Meshkov, Instability of the interface of two gases accelerated by a shock wave, Fluid Dyn. 4 (5) (1969) 101.
[31] H. Duan, C.S. Wu, W.B. Pei, S.Y. Zou, Theoretical study of symmetry of flux onto a capsule, Phys. Plasmas 22 (2015) 092704.
[32] D.S. Clark, C.R. Weber, V.A. Smalyuk, H.F. Robey, A.L. Kritcher, et al., Mitigating the impact of hohlraum asymmetries in National Ignition Facility implosions using capsule shims, Phys. Plasmas 23 (2016) 072707.
[33] J.F. Gu, Z.S. Dai, P. Song, S.Y. Zou, W.H. Ye, Asymmetric-shell ignition capsule design to tune the low-mode asymmetry during the peak drive, Phys. Plasmas 23 (2016) 082703.
[34] K. Lan, J. Liu, D.X. Lai, W.D. Zheng, X.T. He, High flux symmetry of the spherical hohlraum with octahedral 6LEHs at the hohlraum-to-capsule radius ratio of 5.14, Phys. Plasmas 21 (2014) 010704.
[35] K. Lan, W.D. Zheng, Novel spherical hohlraum with cylindrical laser entrance holes and shields, Phys. Plasmas 21 (2014) 090704.
[36] K. Lan, J. Liu, Z.C. Li, X.F. Xie, W.Y. Huo, et al., Progress in octahedral spherical hohlraum study, Matter Radiat. Extrem. 1 (2016) 8.
[37] W.Y. Huo, Z.C. Li, Y.H. Chen, X.F. Xie, K. Lan, et al., First investigation on the radiation field of the spherical hohlraum, Phys. Rev. Lett. 117 (2016) 025002.
[38] D.H. Munro, P.M. Celliers, G.W. Collins, D.M. Gold, L.B. Da Silva, et al., Shock timing technique for the National Ignition Facility, Phys. Plasmas 8 (2001) 2245.
[39] P. Song, C.L. Zhai, S.G. Li, H. Yong, J. Qi, et al., LARED-integration code for numerical simulation of the whole process of the indirect-drive

laser inertial confinement fusion, High Power Laser Part. Beams 27 (2015) 032007.
[40] Z.F. Fan, S.P. Zhu, W.B. Pei, W.H. Ye, M. Li, et al., Numerical investigation on the stabilization of the deceleration phase Rayleigh-Taylor instability due to alpha particle heating in ignition target, EPL 99 (2012) 65003.
[41] Z.F. Fan, X.T. He, J. Liu, G.L. Ren, B. Liu, et al., A wedged-peak pulse design with medium fuel adiabat for indirect-drive fusion, Phys. Plasmas 21 (2014) 100705.
[42] T. Feng, D. Lai, Y. Xu, An artificial-scattering iteration method for calculating multigroup radiation transfer problems, Chin. J. Comput. Phys. 16 (1999) 199.
[43] W.H. Ye, W.Y. Zhang, X.T. He, Stabilization of ablative Rayleigh-Taylor instability due to change of the Atwood number, Phys. Rev. E 65 (2002) 057401.
[44] L.F. Wang, C. Xue, W.H. Ye, Y.J. Li, Destabilizing effect of density gradient on the Kelvin-Helmholtz instability, Phys. Plasmas 16 (2009) 112104.
[45] L.F. Wang, W.H. Ye, Y.J. Li, Interface width effect on the classical Rayleigh-Taylor instability in the weakly nonlinear regime, Phys. Plasmas 17 (2010) 052305.
[46] J.F. Gu, Z.S. Dai, Z.F. Fan, S.Y. Zou, W.H. Ye, et al., A new metric of the low-mode asymmetry for ignition target designs, Phys. Plasmas 21 (2014) 012704.
[47] J.F. Gu, Z.S. Dai, S.Y. Zou, P. Song, W.H. Ye, et al., New tuning method of the low-mode asymmetry for ignition capsule implosions, Phys. Plasmas 22 (2015) 122704.
[48] F.J.D. Serduke, E. Minguez, S.J. Davidson, C.A. Iglesias, Experimental results on line shifts from dense plasmas, J. Quant. Spectrosc. Radiat. Transf. 65 (2000) 527.
[49] Y.S. Li, W.Y. Huo, K. Lan, A novel method for determining the M-band fraction in laser-driven gold hohlraums, Phys. Plasmas 18 (2011) 022701.
[50] J.F. Gu, S.Y. Zou, Y.S. Li, Z.S. Dai, W.H. Ye, Sensitivity study of ignition capsule implosion performance on the hard X-ray spectral distribution of hohlraum, Phys. Plasmas 19 (2012) 122710.
[51] H.F. Robey, T.S. Perry, H.-S. Park, P. Amendt, C.M. Sorce, et al., Experimental measurements of Au M-band flux in indirectly driven double-shell implosions, Phys. Plasmas 12 (2005) 072701.
[52] M.J. May, M.B. Schneider, S.B. Hansen, H.-K. Chung, D.E. Hinkel, et al., X-ray spectral measurements and collisional radiative modeling of hot, high-Z plasmas at the OMEGA laser, High Energy Density Phys. 4 (2008) 78–87.
[53] G.I. Bell, Taylor Instability on Cylinders and Spheres in the Small Amplitude Approximation, Los Alamos Scientific Laboratory, Report No. LA-1321, 1951.
[54] M.S. Plesset, On the stability of fluid flows with spherical symmetry, J. Appl. Phys. 25 (1954) 96.
[55] A.L. Velikovich, P.F. Schmit, Bell-Plesset effects in Rayleigh-Taylor instability of finite-thickness spherical and cylindrical shells, Phys. Plasmas 22 (2015) 122711.
[56] L.F. Wang, J.F. Wu, H.Y. Guo, W.H. Ye, J. Liu, et al., Weakly nonlinear Bell-Plesset effects for a uniformly converging cylinder, Phys. Plasmas 22 (2015) 082702.